



Article

# High-Stability WSe<sub>2</sub> Homojunction Photodetectors via Asymmetric Schottky and PIN Architectures

Jiaji Yang <sup>1,2,3,4</sup>, Xin Li <sup>1,2,3,4,\*</sup>, Junzhe Gu <sup>2,4</sup>, Feilong Yu <sup>2</sup>, Jin Chen <sup>2</sup>, Wei Lu <sup>1,2,3,4,5</sup>

- Shanghai Research Center for Quantum Sciences, 99 Xiupu Road, Shanghai 201315, China; yangjj2022@shanghaitech.edu.cn (J.Y.); luwei@mail.sitp.ac.cn (W.L.)
- State Key Laboratory of Infrared Physics, Shanghai Institute of Technical Physics, Chinese Academy of Sciences, 500 Yu-Tian Road, Shanghai 200083, China; gujunzhe23@mails.ucas.ac.cn (J.G.); yufeilong@mail.sitp.ac.cn (F.Y.); chenjin@mail.sitp.ac.cn (J.C.)
- School of Physical Science and Technology, ShanghaiTech University, Shanghai 201210, China
- <sup>4</sup> University of Chinese Academy of Sciences, No. 19A Yuquan Road, Beijing 100049, China
- Hangzhou Institute for Advanced Study, University of Chinese Academy of Sciences, No.1 Sub-Lane Xiangshan, Hangzhou 310024, China
- \* Correspondence: lixin4@shanghaitech.edu.cn (X.L.); xschen@mail.sitp.ac.cn (X.C.)

**Abstract:** High-stability photovoltaic devices are crucial for low-power or passive applications in fields such as renewable energy, wearable electronics, and deep-space exploration. However, achieving stable and controllable doping in two-dimensional (2D) materials remains challenging, hindering the optimization of photovoltaic performance. Here, we fabricate three high-performance, self-driven photodetectors based on layered WSe<sub>2</sub> with varying doping concentrations. By leveraging asymmetric Schottky barriers and introducing a defect-free, high-bandgap intrinsic region with a long mean free path, we construct a positive–intrinsic–negative (PIN) vertical homojunction that significantly enhances the photogenerated voltage, photon absorption, and carrier transport efficiency. The resulting PIN junction exhibits a photogenerated voltage of up to 0.58 V, a responsivity of 0.35 A/W, and an external quantum efficiency of 83.9%. Moreover, it maintains a reverse saturation current as low as 0.2 nA at 430 K. These results provide a promising route toward the development of high-responsivity, high-stability van der Waals devices and highlight the potential for 2D material-based technologies to operate reliably under extreme conditions.

Keywords: photovoltaic; two-dimensional materials; homojunction; external quantum efficiency



Academic Editors: Dimitrios Tasis and Choongik Kim

Received: 20 January 2025 Revised: 19 February 2025 Accepted: 3 March 2025 Published: 4 March 2025

Citation: Yang, J.; Li, X.; Gu, J.; Yu, F.; Chen, J.; Lu, W.; Chen, X. High-Stability WSe<sub>2</sub> Homojunction Photodetectors via Asymmetric Schottky and PIN Architectures. Coatings 2025, 15, 301. https:// doi.org/10.3390/coatings15030301

Copyright: © 2025 by the authors. Licensee MDPI, Basel, Switzerland. This article is an open access article distributed under the terms and conditions of the Creative Commons Attribution (CC BY) license (https://creativecommons.org/licenses/by/4.0/).

# 1. Introduction

Amidst the rapidly expanding photovoltaic industry, an unprecedented energy transformation is underway. Photovoltaic (PV) technology, known for its cleanliness and sustainability, has evolved from small-scale demonstration projects to become a fundamental part of the global energy infrastructure [1,2]. However, as conventional PV materials, particularly silicon (Si) solar cells, approach their performance thresholds, the need for novel materials capable of delivering higher efficiency and stability has intensified [3]. Silicon solar cells are known for their mature technology, reliable performance, and impressive photoelectric conversion efficiencies. Nevertheless, the substantial manufacturing costs and energy consumption associated with their production hinder their widespread adoption [4]. Against this backdrop, two-dimensional materials [5] and perovskites [6], with their unique structural and functional properties, have emerged as promising candidates for the next generation of PV devices. Nonetheless, perovskites continue to suffer from

Coatings 2025, 15, 301 2 of 10

stability issues [7], prompting increased attention toward 2D materials as more robust alternatives.

Consisting of atomically thin layers, 2D materials, which feature a large surface area, tunable band structures, and excellent optoelectronic properties, are highly appealing for PV applications [8]. Herein, transition metal dichalcogenides (TMDs) [9–12], such as MoS<sub>2</sub> and WSe<sub>2</sub>, exhibit strong light–matter interactions and significant photocatalytic potential [13–18]. These diverse capabilities afford 2D materials considerable promise in enhancing the photoelectric conversion efficiency of PV devices, as well as broad applicability in fields like photocatalysis [19] and optical sensing [20,21]. However, the lack of precisely controllable doping techniques in two-dimensional materials makes it challenging to optimize the band structure of homojunction photovoltaic devices in a manner similar to that for siliconbased or perovskite materials [22,23]. This limitation partially restricts the application of TMDs. The introduction of interlayer interfaces results in low responsivity, rapid carrier recombination, and limited environmental stability [24,25]. Consequently, improving photoelectric conversion efficiency via sophisticated band engineering and device architecture optimization remains a principal challenge.

In this work, we propose an enhanced WSe<sub>2</sub> homojunction photovoltaic device that capitalizes on the combined effects of asymmetric Schottky barriers and a PIN junction. By systematically validating the photovoltaic characteristics of Schottky and PN junctions, we integrate these elements into a PIN junction with matched energy bands. The resulting structure features a wide bandgap, a high mean free path for photogenerated carriers, and multiple co-directional built-in electric fields, substantially reducing non-equilibrium carrier recombination and thereby elevating the photogenerated electromotive force. Through contact engineering to further optimize absorption, our device achieves an open-circuit voltage as high as 0.58 V, a responsivity of 0.35 A/W, and an external quantum efficiency of 83.9%. Notably, it also demonstrates excellent high-temperature stability. This work provides crucial theoretical and technical support for developing flexible electronics, wearable devices, solar cells, and sensors designed to operate in extreme environments [26,27].

### 2. Methods

#### 2.1. Device Fabrication

Few-layer WSe $_2$  flakes were extracted from commercial bulk crystals using mechanical exfoliation. The flakes were then transferred to a silicon substrate with a 285 nm silicon dioxide layer using polydimethylsiloxane (PDMS) in sequence and stacked to form a van der Waals junction. For the preparation of metal electrodes, the photoresist was first spin-coated, and the electrode pattern was defined using a laser direct-write system. The electrodes were deposited via electron beam evaporation with a base pressure of  $8 \times 10^{-7}$  Torr and a deposition rate of 0.2 Å/s. The standard lift-off process was subsequently performed, repeating the steps to complete the fabrication of asymmetric electrodes.

#### 2.2. Device Characterization

All tests were conducted at room temperature (300 K) in an atmospheric environment. The morphology and dimensions of the exfoliated WSe<sub>2</sub> flakes and fabricated devices were verified using a Zeiss Lab5 optical microscope. Electrical measurements were performed using a Keysight B2912 source meter, while optoelectronic performance was characterized by directly illuminating the device surface with a single-wavelength laser at different biases. The optical power density was determined using a photometer.

Coatings 2025, 15, 301 3 of 10

#### 2.3. DFT Simulations

The band structures of both intrinsic and doped WSe $_2$  were simulated using Materials Studio (Accelrys) and CASTEP programs based on density functional theory (DFT). In this study, four-layer WSe $_2$  supercell structures were established, and this model underwent structural optimization with gradient-corrected functionals and utilized perfectly matched basis sets [28]. Structural optimization convergence was set to "Fine", with thresholds of  $5.0 \times 10^{-6}$  eV/atom for energy, 0.01 eV/Å for force, 0.02 GPa for stress, and  $5.0 \times 10^{-4}$  Å for displacement.

#### 3. Results and Discussion

WSe<sub>2</sub> is a representative transition metal dichalcogenide with a hexagonal crystal structure (space group: P63/mmc) and a typical layered arrangement. The layers are held together by van der Waals forces, with tungsten atoms positioned between selenium atoms, forming strong chemical bonds. The structure shows a hexagonal close-packed (HCP) arrangement, as depicted in Figure 1a. Monolayer WSe<sub>2</sub> has a direct bandgap of approximately 1.6 eV [29], while thicker layers exhibit an indirect bandgap of around 1.2 eV to 1.3 eV [30] (Figure 1b). The bandgap is close to the Shockley–Queisser limit [31], where most of the photon energy in the solar spectrum can be efficiently absorbed with low thermalization losses. Therefore, WSe<sub>2</sub> is an ideal material for single-junction photovoltaic cells, achieving optimal light absorption efficiency. In addition, WSe<sub>2</sub> exhibits a relatively mature doping process, unlike materials such as MoS<sub>2</sub>, which tend to introduce sulfur vacancies during growth, leading to uncertain doping [22,25]. Thus, the optical absorption characteristics of intrinsic WSe<sub>2</sub> were initially explored.

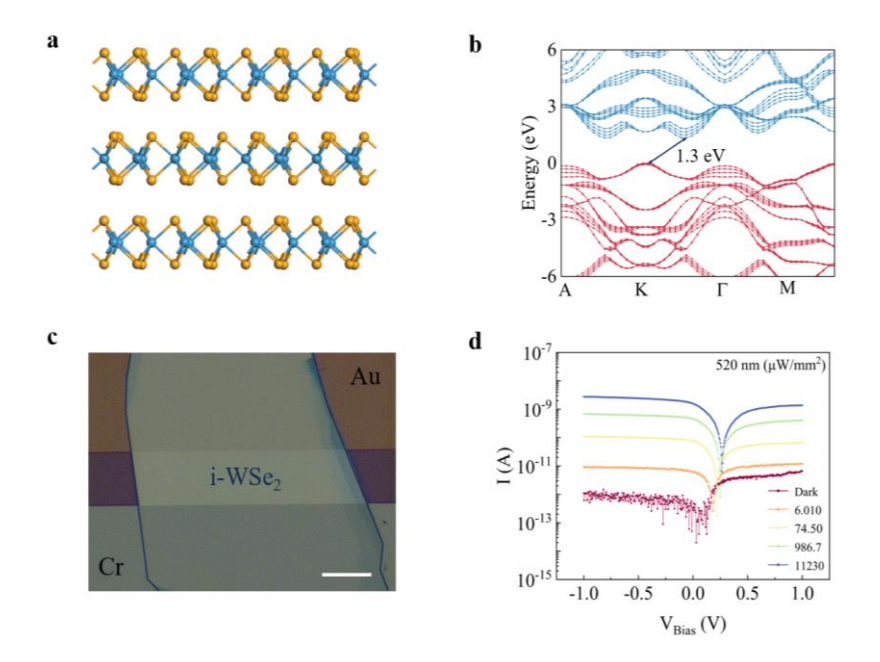


Figure 1. The structure of WSe<sub>2</sub> and the performance characterization of its Schottky diodes. (a) Crystal structure of intrinsic WSe<sub>2</sub>, with orange spheres representing Se atoms and blue spheres representing W atoms. (b) Band structure of intrinsic WSe<sub>2</sub>. (c) Optical microscope image of a  $Cr/WSe_2/Au$  photovoltaic device with asymmetric electrodes; scale bar 10  $\mu$ m. (d) I–V characteristics of the device under different optical power densities.

As shown in Figure 1c, a photovoltaic structure with asymmetric electrodes was fabricated using intrinsic WSe<sub>2</sub>. The structure generates an internal electric field at the metal–semiconductor interfaces. One side of the WSe<sub>2</sub> contacts Au, creating p-type doping, while the other side contacts Cr, creating n-type doping, forming a PIN junction [16,32]. The

Coatings 2025, 15, 301 4 of 10

device's optoelectronic response is shown in Figure 1d. The Schottky junction suppresses the reverse leakage current to below 1 pA in the dark. However, due to the low conductivity of the intrinsic semiconductor, the forward conduction current remains low. Under 520 nm light illumination, a clear photocurrent and photovoltage are observed. The two Schottky barriers in the WSe<sub>2</sub>'s space charge region create accumulation zones, which are narrow and allow for the recombination of the photogenerated carriers, reducing light absorption efficiency. As a result, the maximum short-circuit current is 1.57 nA, and the maximum photovoltage is 0.27 V.

The homojunction PN junction can effectively address issues related to low semiconductor interface states and the accumulation region [9]. Asymmetric electrodes enhance the performance of the depletion region in PN junctions, as shown in Figure 2a. Thin layers of n-type WSe<sub>2</sub> (Re-doped) and p-type WSe<sub>2</sub> (Nb-doped) were stacked on an SiO<sub>2</sub> substrate to form a vertical junction using mechanical transfer. The electrode positions were defined based on a standard photolithography process, followed by electron beam evaporation of Cr to contact the n-type WSe<sub>2</sub> and Au to contact the p-type WSe<sub>2</sub>. The device's optical microscope image is shown in Figure 2b. Additionally, Figure 2c shows the band diagram of the device, where the diffusion and drift currents in the PN junction balance to generate an internal electric field. Due to the alignment of the band structure in the homojunction, the issue of barrier spikes in the heterojunctions is effectively mitigated [10]. Although the Fermi level pinning effect of doped materials can lead to a reduction in the Schottky barrier, the asymmetric Schottky junction and the internal electric field of the PN junction further enhance rectification and carrier separation.

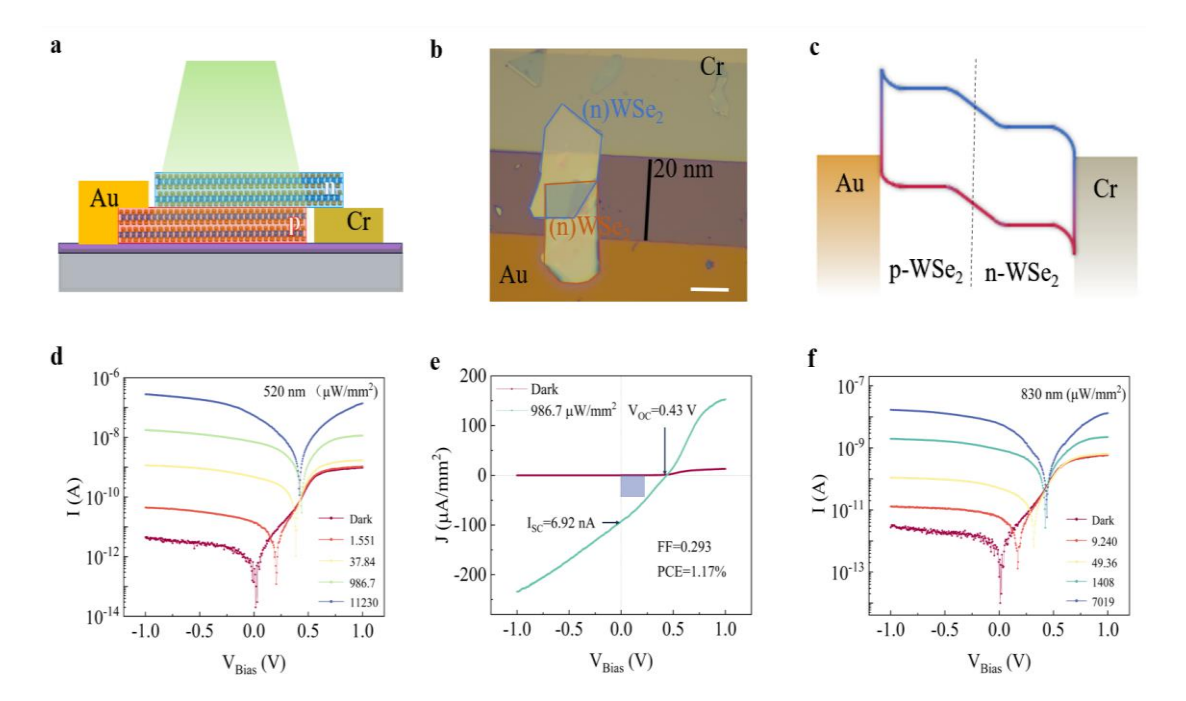


Figure 2. Structure and photoelectric response of the Au/(p)WSe<sub>2</sub>/(n)WSe<sub>2</sub>/Cr photovoltaic device. (a) Schematic diagram of the device structure. (b) Optical microscope image of the device; scale bar  $10~\mu m$ . (c) Band structure of the device. (d) I–V characteristics of the device under 520 nm illumination with different optical power densities. (e) Response characterization of the device in the dark and under illumination, demonstrating the diode's self-driving effect. (f) I–V characteristics of the device in the dark and under 830 nm illumination.

As shown in Figure 2d, the reverse leakage current in the dark state of the structure slightly increases, which could be due to recombination or tunneling effects caused by impurity states. However, the doping PN junction significantly improves the rectification

Coatings 2025, 15, 301 5 of 10

ratio, reaching approximately 217 times. Additionally, under 520 nm illumination, the device achieves a maximum photogenerated voltage of 0.43 V, with the short-circuit current increasing to 54 nA.

To further demonstrate the application potential of our device, its self-driving effect under intensities of 986.7  $\mu$ W/mm² illumination at 520 nm is shown in Figure 2e. The device achieves a fill factor of 0.293 and a photovoltaic conversion efficiency of about 1.17%. This result clearly demonstrates the potential application of the enhanced PN homojunction. Furthermore, the device's performance was tested under different bias voltages and 830 nm illumination. Despite the photon energy being close to the WSe<sub>2</sub> bandgap, the device shows remarkable near-infrared light detection potential, with a responsivity of 36.8 mA/W at zero bias.

To investigate the influence of different structures on device performance, another enhanced PIN vertical structure was designed [33–35], as shown in Figure 3a. The p-type, i-type, and n-type layered  $WSe_2$  materials were stacked to form a vertical junction, and the device's optical microscope image is shown in Figure 3b. The built-in potential barrier heights at both ends of the PIN structure are equivalent to those of the PN junction, due to the consistent effect of the same doped materials on the Fermi level. However, because of minimal doping in the intrinsic region, the space charge region becomes wider, according to Poisson's equation, increasing the light absorption area.

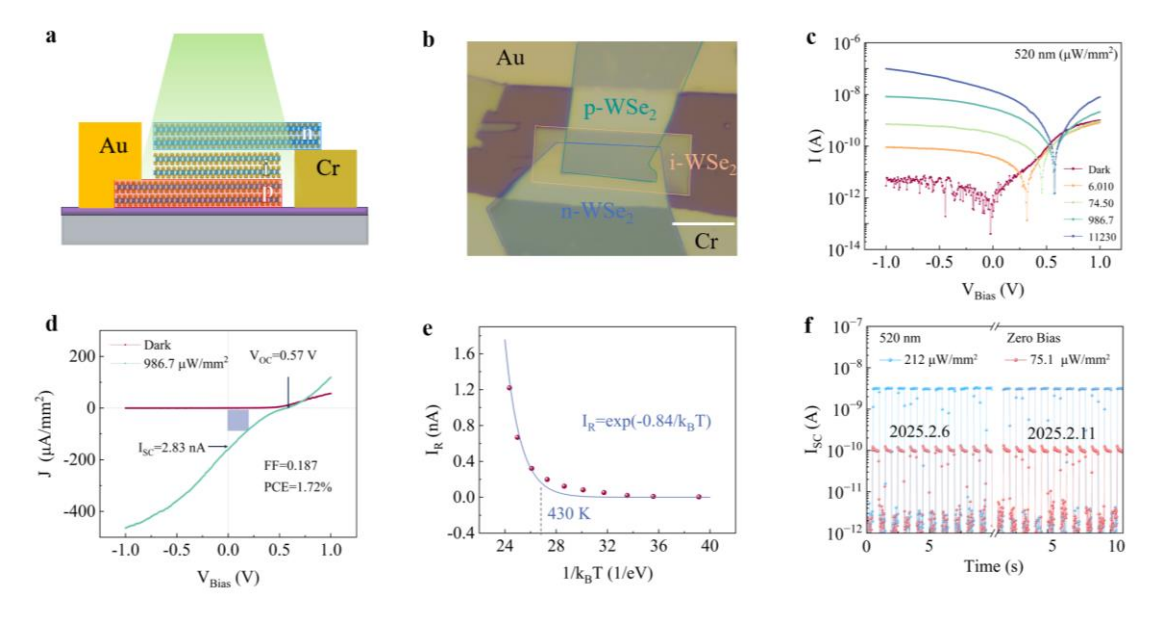


Figure 3. Structure and photoelectric response of the  $Au/(p)WSe_2/(i)WSe_2/(n)WSe_2/Cr$  photovoltaic device. (a) Schematic diagram of the device structure. (b) Optical microscope image of the device; scale bar 5  $\mu$ m. (c) I–V characteristics of the device under 520 nm illumination with different optical power densities. (d) Response characterization of the device in the dark and under illumination, demonstrating the diode's self-driving effect. (e) High-temperature I–V response characteristics of the diode. (f) Stability of the PIN device response under pulsed light modulation.

Further characterization of the device's I–V curves under different optical power density was performed. The PIN structure exhibited rectification behavior similar to the PN junction in the dark state, due to the identical built-in electric field and Schottky contact, which resulted in comparable carrier transport behavior. As shown in Figure 3c, under 520 nm illumination, the device exhibited a remarkable photogenerated voltage of 0.58 V. Furthermore, under the same optical power density, the short-circuit current density increases. However, due to the expansion of the depletion region, the fill factor of the PIN junction decreases, and optimizing the width of the intrinsic region can improve

Coatings 2025, 15, 301 6 of 10

this issue. As shown in Figure 3d, the PCE of the PIN junction reached 1.72%, significantly higher than the 1.17% of the PN junction. We will discuss this further in the next section.

Environmental adaptability refers to the stability and reliability of the photodetector in various working environments, which determines its practicality. Under air oxidation, a thin tungsten oxide (WO<sub>3</sub>) layer may form on the surface of WSe<sub>2</sub>, partially protecting it from further oxidation and giving WSe<sub>2</sub> strong atmospheric adaptability [36,37]. Our unencapsulated WSe<sub>2</sub> homojunction exhibited consistent response characteristics, before and after being placed in an atmospheric environment for 5 days, confirming this viewpoint. Additionally, the device's high-temperature tolerance was explored. The rectification characteristics of the device were tested from 300 K to 480 K, and the reverse leakage current of the device did not significantly increase with temperature. As shown in Figure 3e, under a reverse bias of -1 V, the device maintained a low reverse saturation leakage current of less than 0.2 nA at temperatures below 430 K. This is partly due to the structural stability provided by the dense WSe<sub>2</sub> structure and partly due to the intrinsic layer in the PIN junction, which effectively suppresses carrier recombination and tunneling effects with its undoped, electrically neutral structure. Excessive carrier recombination and thermal excitation are suppressed at high temperatures, demonstrating the device's detection potential in extreme environments.

# 4. Discussion of PN and PIN Junction

To further explore the internal mechanisms underlying the performance differences between the PIN and PN structures, we analyze both the photogenerated voltage and photoresponse characteristics. When photons with energy greater than the bandgap are incident, they drive the device into a non-equilibrium state. Electrons in the conduction band and holes in the valence band are each in a "quasi-equilibrium state". As the light intensity increases, the difference between the quasi-Fermi levels of the electrons and holes also increases, leading to a larger photogenerated voltage. However, the difference is capped by the material's bandgap [31]. As shown in Figure 4a,b, when doped with Re, additional impurity levels—especially those associated with the d-orbitals of Re—may be introduced. These levels interact with the valence and conduction bands of WSe<sub>2</sub>, reducing the bandgap size. In the case of Nb doping, a significant number of acceptor levels are clearly introduced near the valence band maximum, reducing the bandgap to 1.1 eV at this doping concentration.

However, factors such as carrier recombination, interface defects, and incomplete charge separation result in a reduction in the actual upper limit of the photogenerated voltage. In the PN structure, as shown in Figure 4c, photogenerated carriers are mainly generated and separated in the space charge region. However, since the semiconductor interface is located in the middle of the region, photogenerated carriers are subject to significant recombination at the interface due to defect states. Furthermore, the collection process of photogenerated carriers in the PN junction is limited by minority carrier diffusion and is prone to being trapped by ions in the space charge region. Therefore, Shockley-Read-Hall (SRH) recombination and Auger recombination are the primary limiting factors for photogenerated carrier collection in the PN junction [38]. In contrast, in the PIN structure, photogenerated carriers are primarily absorbed and separated in the intrinsic region, forming drift currents [35]. The mechanism significantly reduces the impact of interface defects and ions, as shown in Figure 4d. In addition, while the intrinsic region benefits from higher carrier mobility, it also increases the transport distance of carriers, thereby raising the probability of carrier recombination. Therefore, reasonable doping concentrations and structural adjustments can promote better carrier collection.

Coatings 2025, 15, 301 7 of 10

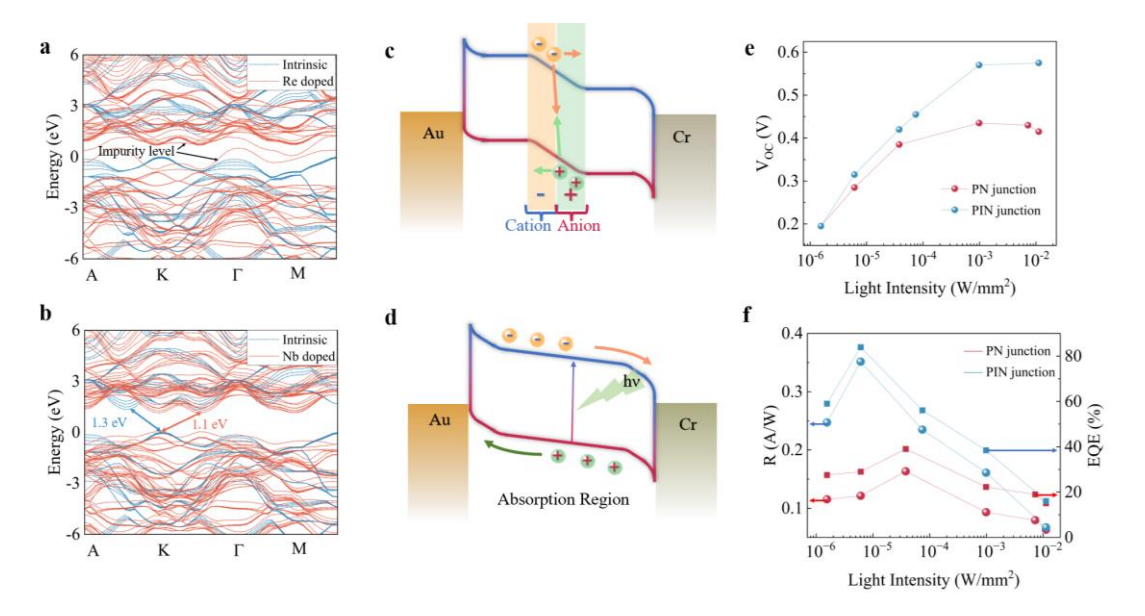


**Figure 4. Comparison of Response Mechanisms and Performance of PN and PIN Junctions.** The band structures of n-type WSe<sub>2</sub> (Re-doped) (**a**) and p-type WSe<sub>2</sub> (Nb-doped) (**b**) are shown. The energy band diagrams and carrier transport mechanisms for PN junction (**c**) and PIN junction (**d**) devices. A comparison of the PN junction and PIN junction under different optical power conditions is presented in terms of open-circuit voltage (**e**), responsivity, and external quantum efficiency (**f**) with varying optical power densities at zero bias.

In summary, the PIN structure not only offers a higher upper limit for the photogenerated voltage but also exhibits higher carrier collection efficiency, resulting in reduced open-circuit voltage losses. Therefore, under the same optical power, the photogenerated electromotive force of the PIN diode is larger, as shown in Figure 4e. Additionally, the PIN structure's larger absorption region results in a higher absorption rate, along with improved carrier collection efficiency. As shown in Figure 4f and Table 1, the PIN structure exhibits higher responsivity, especially at low power, with a responsivity of 0.35 A/W, an external quantum efficiency of 83.9%, and a detectivity of  $2.37 \times 10^{11}$  cm  $Hz^{1/2}W^{-1}$ , based on the formulas R = I/PA,  $EQE = I/Ph\nu$ ,  $D^* = A^{1/2}R/(2eI_d)^{1/2}$ . Herein, I is the photocurrent at zero bias, P is the optical power density, A is the effective area of the device, h is Planck's constant,  $\nu$  is the frequency, e is the elementary charge, and  $I_d$  is the dark current.

Table 1. Performance	e of some recent t	wo-dimensional	l material se	lf-driven ph	notodetectors
<b>Table 1.</b> I ellolinalice	e of some recent t	.wo-umiensionai	i illateriai se	m-univen bi	ioiodeleciois.

Structure	Max V <sub>oc</sub> (V)	R (A/W)	EQE (%)
ITO/WSe <sub>2</sub> /Au [39]	0.38	~0.1	/
$(p)MoSe_2/(n)MoSe_2$ [9]	0.35	~0.18	~50
Double-Gate MoTe <sub>2</sub> [11]	0.32	/	~40
Thick WSe <sub>2</sub> /Thin WSe <sub>2</sub> [17]	0.49	0.112	/
$Gd/WSe_2/Pt$ [18]	0.34	/	/
Thick MoTe <sub>2</sub> /Thin MoTe <sub>2</sub> [10]	0.21	~0.6	/
Double-Gate MoTe <sub>2</sub> [12]	0.31	0.015	4.68
(p)BP/(n)BP [23]	0.14	0.006	/
$Pd/(p)WSe_2/Ti$ [40]	0.8	~0.2	/
This work	0.58	0.35	83.9

## 5. Conclusions

In summary, we have demonstrated three types of self-powered photodetectors based on layered WSe<sub>2</sub>, leveraging asymmetric Schottky barriers and homojunction architectures.

Coatings 2025, 15, 301 8 of 10

By systematically examining devices with intrinsic WSe<sub>2</sub> (Schottky), PN junctions, and PIN junctions, we identified the PIN configuration as the most effective approach for improving photogenerated voltage, reducing carrier recombination, and enhancing responsivity. Notably, the PIN device achieved a photovoltage of 0.58 V, a responsivity of 0.35 A/W, and an EQE of 83.9%, along with excellent thermal stability up to 430 K. These improvements stem from the inclusion of a wide intrinsic layer that extends the depletion region, thereby boosting light absorption and carrier transport efficiency. Overall, our findings not only shed light on the underlying carrier dynamics in WSe<sub>2</sub>-based van der Waals junctions but also offer a practical route toward high-performance, flexible, and thermally stable photovoltaics and photodetectors.

**Author Contributions:** Conceptualization, X.L. and J.Y.; methodology, J.C. and F.Y.; software, J.Y.; validation, J.Y., X.L. and J.G.; formal analysis, J.Y. and X.L.; investigation, J.G.; resources, X.C. and W.L.; data curation, J.Y. and X.L.; writing—original draft preparation, J.Y.; writing—review and editing, X.C. and X.L.; visualization, J.Y.; supervision, X.C. and X.L.; project administration, W.L. and X.C.; funding acquisition, X.C. All authors have read and agreed to the published version of the manuscript.

Funding: This work was supported by National Key Research and Development Program of China (2023YFA1406900); Strategic Priority Research Program (B) of Chinese Academy of Sciences (XDB0580000, GJ0090406); National Natural Science Foundation of China (62222514, 62350073, U2341226, 12227901); Shanghai Science and Technology Committee (23ZR1482000, 22JC1402900); Shanghai Municipal Science and Technology Major Project (2019SHZDZX01); Natural Science Foundation of Zhejiang Province (LR22F050004); Youth Innovation Promotion Association (Y2021070) and International Partnership Program (112GJHZ2022002FN) of Chinese Academy of Sciences. This work was partially carried out in Soft Matter Nanofab (SMN180827) in ShanghaiTech University.

**Data Availability Statement:** Relevant data supporting the key findings of this study are available in the article. All raw data generated in this study are available from the corresponding author upon reasonable request.

**Conflicts of Interest:** The authors declare no competing interests.

#### References

- 1. Polman, A.; Knight, M.; Garnett, E.C.; Ehrler, B.; Sinke, W.C. Photovoltaic materials: Present efficiencies and future challenges. *Science* **2016**, *352*, aad4424. [CrossRef]
- 2. Wang, Y.; Wang, R.; Tanaka, K.; Ciais, P.; Penuelas, J.; Balkanski, Y.; Sardans, J.; Hauglustaine, D.; Liu, W.; Xing, X.; et al. Accelerating the energy transition towards photovoltaic and wind in China. *Nature* **2023**, *619*, 761–767. [CrossRef] [PubMed]
- 3. Okil, M.; Salem, M.S.; Abdolkader, T.M.; Shaker, A. From Crystalline to Low-cost Silicon-based Solar Cells: A Review. *Silicon* **2022**, *14*, 1895–1911. [CrossRef]
- 4. Mao, D.; Yang, S.; Ma, L.; Ma, W.; Yu, Z.; Xi, F.; Yu, J. Overview of life cycle assessment of recycling end-of-life photovoltaic panels: A case study of crystalline silicon photovoltaic panels. *J. Clean. Prod.* **2024**, 434, 140320. [CrossRef]
- 5. Yu, H.; Wang, Y.; Zeng, H.; Cao, Z.; Zhang, Q.; Gao, L.; Hong, M.; Wei, X.; Zheng, Y.; Zhang, Z.; et al. High-Spike Barrier Photodiodes Based on 2D Te/WS2 Heterostructures. *ACS Nano* **2024**, *18*, 17100–17110. [CrossRef] [PubMed]
- 6. Liu, S.; Li, J.; Xiao, W.; Chen, R.; Sun, Z.; Zhang, Y.; Lei, X.; Hu, S.; Kober-Czerny, M.; Wang, J.; et al. Buried interface molecular hybrid for inverted perovskite solar cells. *Nature* **2024**, *632*, 536–542. [CrossRef]
- 7. Li, G.; Su, Z.; Canil, L.; Hughes, D.; Aldamasy, M.H.; Dagar, J.; Trofimov, S.; Wang, L.; Zuo, W.; Jerónimo-Rendon, J.J.; et al. Highly efficient p-i-n perovskite solar cells that endure temperature variations. *Science* **2023**, *379*, 399–403. [CrossRef]
- 8. Zhang, Y.; Wu, J.; Jia, L.; Jin, D.; Jia, B.; Hu, X.; Moss, D.; Gong, Q. Advanced optical polarizers based on 2D materials. *NPJ Nanophotonics* **2024**, *1*, 28. [CrossRef]
- 9. Jin, Y.; Keum, D.H.; An, S.-J.; Kim, J.; Lee, H.S.; Lee, Y.H. A Van Der Waals Homojunction: Ideal p–n Diode Behavior in MoSe<sub>2</sub>. *Adv. Mater.* **2015**, 27, 5534–5540. [CrossRef]
- 10. Wen, P.; Zhang, L.; Gao, W.; Yue, Q.; Wang, H.; Huang, Y.; Wu, J.; Yu, H.; Chen, H.; Huo, N.; et al. Gate-Tunable Photovoltaic Effect in MoTe<sub>2</sub> Lateral Homojunction. *Adv. Electron. Mater.* **2022**, *8*, 2101144. [CrossRef]

Coatings 2025, 15, 301 9 of 10

11. Wu, G.; Wang, X.; Chen, Y.; Wu, S.; Wu, B.; Jiang, Y.; Shen, H.; Lin, T.; Liu, Q.; Wang, X.; et al. MoTe<sub>2</sub> p–n Homojunctions Defined by Ferroelectric Polarization. *Adv. Mater.* **2020**, 32, 1907937. [CrossRef] [PubMed]

- 12. Cheng, L.; Yu, J.; Wei, Y.; Feng, Z.; Li, Y.; Wang, Y.; Xu, N.; Wang, Z.L.; Sun, Q. Triboelectric-potential configurable MoTe<sub>2</sub> homojunction for photovoltaic device and logic circuits. *Nano Energy* **2023**, *114*, 108632. [CrossRef]
- 13. Kumar, K.; Kaur, D. A review on recent advancements in the growth of MoS<sub>2</sub> based flexible photodetectors. *Sol. Energy Mater. Sol. Cells* **2024**, *268*, 112736. [CrossRef]
- 14. Wu, W.; Liu, Z.; Qiu, Z.; Wu, Z.; Li, Z.; Yang, X.; Han, L.; Li, C.; Huo, N.; Wang, X.; et al. An Ultrasensitive ReSe<sub>2</sub>/WSe<sub>2</sub> Heterojunction Photodetector Enabled by Gate Modulation and its Development in Polarization State Identification. *Adv. Opt. Mater.* 2024, 12, 2301410. [CrossRef]
- 15. Deng, W.; Zheng, Z.; Li, J.; Zhou, R.; Chen, X.; Zhang, D.; Lu, Y.; Wang, C.; You, C.; Li, S.; et al. Electrically tunable two-dimensional heterojunctions for miniaturized near-infrared spectrometers. *Nat. Commun.* **2022**, *13*, 4627. [CrossRef]
- 16. Kong, L.; Zhang, X.; Tao, Q.; Zhang, M.; Dang, W.; Li, Z.; Feng, L.; Liao, L.; Duan, X.; Liu, Y. Doping-free complementary WSe<sub>2</sub> circuit via van der Waals metal integration. *Nat. Commun.* **2020**, *11*, 1866. [CrossRef]
- 17. Tan, C.; Wang, H.; Zhu, X.; Gao, W.; Li, H.; Chen, J.; Li, G.; Chen, L.; Xu, J.; Hu, X.; et al. A Self-Powered Photovoltaic Photodetector Based on a Lateral WSe<sub>2</sub>-WSe<sub>2</sub> Homojunction. *ACS Appl. Mater. Interfaces* **2020**, *12*, 44934–44942. [CrossRef]
- 18. Aftab, S.; Hegazy, H.H.; Iqbal, M.Z.; Iqbal, M.W.; Nazir, G.; Hussain, S. Recent Advances in Dynamic Homojunction PIN Diodes Based on 2D Materials. *Adv. Mater. Interfaces* **2023**, *10*, 2201937. [CrossRef]
- 19. Li, Z.; Meng, X.; Zhang, Z. Recent development on MoS<sub>2</sub>-based photocatalysis: A review. *J. Photochem. Photobiol. C Photochem. Rev.* **2018**, 35, 39–55. [CrossRef]
- 20. Dai, M.; Zhang, X.; Wang, Q.J. 2D Materials for Photothermoelectric Detectors: Mechanisms, Materials, and Devices. *Adv. Funct. Mater.* **2024**, *34*, 2312872. [CrossRef]
- 21. Pawar, K.K.; Kumar, A.; Mirzaei, A.; Kumar, M.; Kim, H.W.; Kim, S.S. 2D nanomaterials for realization of flexible and wearable gas sensors: A review. *Chemosphere* **2024**, *352*, 141234. [CrossRef] [PubMed]
- 22. Liu, Y.; Guo, J.; Zhu, E.; Liao, L.; Lee, S.-J.; Ding, M.; Shakir, I.; Gambin, V.; Huang, Y.; Duan, X. Approaching the Schottky–Mott limit in van der Waals metal–semiconductor junctions. *Nature* **2018**, *557*, 696–700. [CrossRef] [PubMed]
- 23. Liu, Y.; Cai, Y.; Zhang, G.; Zhang, Y.-W.; Ang, K.-W. Al-Doped Black Phosphorus p–n Homojunction Diode for High Performance Photovoltaic. *Adv. Funct. Mater.* **2017**, 27, 1604638. [CrossRef]
- 24. Hou, X.; Jin, T.; Zheng, Y.; Chen, W. Atomic-scale interface engineering for two-dimensional materials based field-effect transistors. SmartMat 2024, 5, e1236. [CrossRef]
- 25. Yang, J.; Bussolotti, F.; Kawai, H.; Goh, K.E.J. Tuning the Conductivity Type in Monolayer WS2 and MoS<sub>2</sub> by Sulfur Vacancies. *Phys. Status Solidi RRL-Rapid Res. Lett.* **2020**, *14*, 2000248. [CrossRef]
- 26. Pasupuleti, K.S.; Reddeppa, M.; Park, B.-G.; Peta, K.R.; Oh, J.-E.; Kim, S.-G.; Kim, M.-D. Ag Nanowire-Plasmonic-Assisted Charge Separation in Hybrid Heterojunctions of Ppy-PEDOT:PSS/GaN Nanorods for Enhanced UV Photodetection. *ACS Appl. Mater. Interfaces* **2020**, *12*, 54181–54190. [CrossRef]
- 27. Sun, B.; Xu, G.; Ji, X.; Yang, Z.; Guan, C.; Chen, S.; Chen, X.; Ma, Y.; Yu, Y.; Feng, J. A strain-resistant flexible thermistor sensor array based on CNT/MXene hybrid materials for lithium-ion battery and human temperature monitoring. *Sens. Actuators A Phys.* **2024**, *368*, 115059. [CrossRef]
- 28. Perdew, J.P.; Burke, K.; Ernzerhof, M. Generalized Gradient Approximation Made Simple. *Phys. Rev. Lett.* **1996**, 77, 3865–3868. [CrossRef]
- 29. Xiao, J.; Zhang, Y.; Chen, H.; Xu, N.; Deng, S. Enhanced Performance of a Monolayer MoS<sub>2</sub>/WSe<sub>2</sub> Heterojunction as a Photoelectrochemical Cathode. *Nano-Micro Lett.* **2018**, *10*, 60. [CrossRef]
- 30. Kim, K.; Larentis, S.; Fallahazad, B.; Lee, K.; Xue, J.; Dillen, D.C.; Corbet, C.M.; Tutuc, E. Band Alignment in WSe<sub>2</sub>–Graphene Heterostructures. *ACS Nano* **2015**, *9*, 4527–4532. [CrossRef]
- 31. Nayak, P.K.; Mahesh, S.; Snaith, H.J.; Cahen, D. Photovoltaic solar cell technologies: Analysing the state of the art. *Nat. Rev. Mater.* **2019**, *4*, 269–285. [CrossRef]
- 32. Li, Y.; Xiao, J.; Cao, X.; Gu, Z.; Zhang, W. Lateral WSe<sub>2</sub> Homojunction through Metal Contact Doping: Excellent Self-powered Photovoltaic Photodetector. *Adv. Funct. Mater.* **2023**, *33*, 2213385. [CrossRef]
- 33. Zhang, Y.; Ma, K.; Zhao, C.; Hong, W.; Nie, C.; Qiu, Z.-J.; Wang, S. An Ultrafast WSe<sub>2</sub> Photodiode Based on a Lateral p-i-n Homojunction. *ACS Nano* **2021**, *15*, 4405–4415. [CrossRef] [PubMed]
- 34. Gao, R.; Liu, L.; Li, Y.; Shen, L.; Wan, P.; Ouyang, X.; Zhang, H.; Ruan, J.; Zhou, L.; Chen, L.; et al. High-performance alpha-voltaic cell based on a 4H-SiC PIN junction diode. *Energy Convers. Manag.* **2022**, 252, 115090. [CrossRef]
- 35. Liu, H.; Pasanen, T.P.; Fung, T.H.; Isometsä, J.; Haarahiltunen, A.; Hesse, S.; Werner, L.; Vähänissi, V.; Savin, H. Near-infrared germanium PIN-photodiodes with >1A/W responsivity. *Light Sci. Appl.* **2025**, *14*, 9. [CrossRef]
- 36. Pataniya, P.M.; Yang, X.; Li, B.; Kannichankandy, D.; Sumesh, C.K. Enhanced electrocatalysis of WSe nanosheets by partial oxidation for hydrogen generation. *Int. J. Energy Res.* **2022**, *46*, 12073–12081. [CrossRef]

Coatings 2025, 15, 301 10 of 10

37. Lv, Q.; Tan, J.; Wang, Z.; Gu, P.; Liu, H.; Yu, L.; Wei, Y.; Gan, L.; Liu, B.; Li, J.; et al. Ultrafast charge transfer in mixed-dimensional WO3-x nanowire/WSe<sub>2</sub> heterostructures for attomolar-level molecular sensing. *Nat. Commun.* **2023**, *14*, 2717. [CrossRef]

- 38. Yoon, H.H.; Fernandez, H.A.; Nigmatulin, F.; Cai, W.; Yang, Z.; Cui, H.; Ahmed, F.; Cui, X.; Uddin, M.G.; Minot, E.D.; et al. Miniaturized spectrometers with a tunable van der Waals junction. *Science* **2022**, *378*, 296–299. [CrossRef]
- 39. Luo, M.; Wu, F.; Long, M.; Chen, X. WSe<sub>2</sub>/Au vertical Schottky junction photodetector with low dark current and fast photoresponse. *Nanotechnology* **2018**, 29, 444001. [CrossRef]
- 40. Park, J.; Kim, S.; Yang, M.; Hosono, H.; Park, K.; Yoon, J.; Bak, J.; You, B.; Park, S.-W.; Hahm, M.G.; et al. Nature of Photoconductivity in Self-Powered Single-Atomic-Layered Nb-Doped WSe<sub>2</sub> Phototransistors. *ACS Photonics* **2023**, *10*, 2930–2940. [CrossRef]

**Disclaimer/Publisher's Note:** The statements, opinions and data contained in all publications are solely those of the individual author(s) and contributor(s) and not of MDPI and/or the editor(s). MDPI and/or the editor(s) disclaim responsibility for any injury to people or property resulting from any ideas, methods, instructions or products referred to in the content.